

Effect of Electric Field Gradients on Lipid Monolayer Membranes

Ka Yee C. Lee and Harden M. McConnell

Department of Chemistry, Stanford University, Stanford, California 94305-5080 USA

ABSTRACT Externally applied nonuniform electric fields can strongly affect thermodynamic phases in a lipid monolayer when applied under conditions of temperature, pressure, and composition that are near phase boundaries. Under such conditions nonuniform applied fields can produce or suppress phase separations. Field-induced phase-separated domains have sizes that are in good agreement with calculations. Field gradients can also produce large concentration gradients in binary mixtures just above their critical points. The present work elaborates our earlier studies of these field effects using thermodynamic models of the phase behavior of two-component liquid mixtures. The calculations are of interest in connection with biological membranes that, at the growth temperature, are in a liquid state close to a phase boundary.

INTRODUCTION

Epifluorescence microscopy has been used to observe coexisting two-dimensional liquid phases in binary mixtures of phospholipids and steroids at the air–water interface (Hirshfeld and Seul, 1990; Knobler and Desai, 1992; McConnell, 1991; Möhwald, 1990; Rice and McConnell, 1989; Seul and Sammon, 1990; Subramaniam and McConnell, 1987). Our monolayer studies were initially stimulated by evidence for coexisting liquid phases in bilayers composed of such binary mixtures (Recktenwald and McConnell, 1981; Vist and Davis, 1990) and by the possibility that the coexisting phases might be significant for the structure and function of biological membranes (Linden et al., 1973; Wisnieski and Fox, 1976). Recently, we have used an inhomogeneous electric field to manipulate lipid monolayer domains (Klingler and McConnell, 1993; Lee and McConnell, 1993). This has led to the discovery that modest electrical potentials can give rise to substantial lateral concentration gradients and phase separations in lipid monolayers with compositions and properties that potentially mimic some biological membranes (Lee et al., 1994).

The system under investigation is a binary mixture of dihydrocholesterol (DChol) and dimyristoylphosphatidylcholine (DMPC). This mixture forms two immiscible liquid phases at convenient temperatures and pressures and exhibits a mixing–demixing critical point (Benvegnu and McConnell, 1993). Fig. 1 shows the phase diagram of the DChol–DMPC system recently obtained in this laboratory (Benvegnu and McConnell, 1993; J. P. Hagen and H. M. McConnell, unpublished observations). At a critical composition of ~30% DChol, the two liquid phases, one rich in DChol and the other rich in DMPC, merge into a single phase of uniform composition at the critical point upon increase in lateral pressure. DChol is less susceptible to air oxidation than cholesterol,

but the phase behavior is very similar (Hirshfeld and Seul, 1990; Subramaniam and McConnell, 1987).

The domain sizes and shapes in the liquid–liquid coexistence region have been interpreted phenomenologically in terms of a competition between line tension at the domain boundary and dipole–dipole electrostatic repulsion between molecules within and between the domains (McConnell, 1991). Because of the difference in dipole moment density between the coexisting phases, an electric field gradient tends to separate the phases.

It is important to distinguish carefully between electrical-field-induced phase separations and electric-field-induced separation of phases. For example, in a number of studies it has been shown that inhomogeneous electric fields can be used to electrophorese lipid domains at the air–water interface (Heckl et al., 1988; Klingler and McConnell, 1993; Lee and McConnell, 1993). This electrophoresis thus produces a separation of previously existing phases in a monolayer. An early study of the effects of electrical fields on monolayers by Middleton and Pethica (1981) may have also involved this separation of previously existing phases. In our earlier study (Lee et al., 1994), and in the present work, we are concerned primarily with the effect of an electrical field in producing a phase separation, that is, the induction of a phase separation in a system that is microscopically homogeneous in the absence of the applied field. Our experimental results are interpreted in terms of the thermodynamic properties of the two liquid phases as well as their interactions with the applied field.

EXPERIMENTAL RESULTS

The previous experimental results on electric-field-induced concentration gradients in lipid monolayers are briefly summarized here (Lee et al., 1994).

Binary mixtures of DChol and DMPC with an added 1 mol. % of the dye *N*-(Texas Red sulfonyl)dipalmitoyl-*L*-α-phosphatidylethanolamine were spread on a microfluorescence film balance with a 2-mmol KCl subphase (Benvegnu and McConnell, 1993; Klingler and McConnell, 1993). The dye, which preferentially associates with DMPC, provides

Received for publication 7 November 1994 and in final form 26 January 1995.

Address reprint requests to Dr. Harden M. McConnell, Department of Chemistry, Stanford University, Stanford, California 94305-5080. Tel.: 415-723-4571; FAX: 415-723-4923; E-mail: harden@leland.stanford.edu.

© 1995 by the Biophysical Society
0006-3495/95/05/1740/12 \$2.00

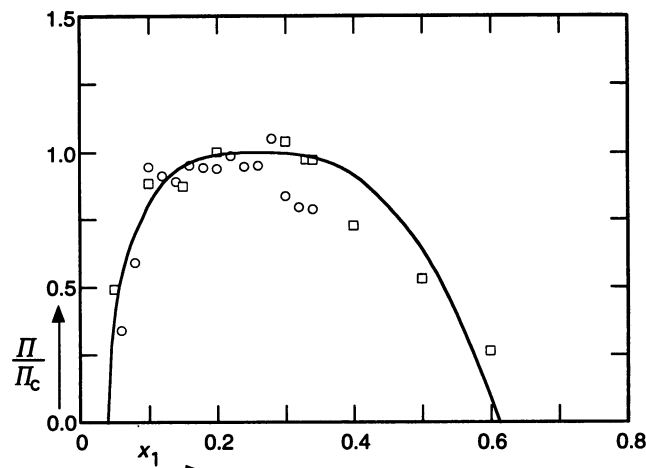


FIGURE 1 Phase diagram for a binary mixture of DChol and DMPC. Pressure Π is measured in units of the critical pressure Π_c , and x_1 is the mole fraction of DChol. Data are taken from Hagen and McConnell (unpublished) (○) and Benvegnù and McConnell (1993) (□). The solid curve is a rough fit to the data. The upper portion of the curve conforms to the functional form $|x_1^{(a)} - x_1^{(b)}|/2x_{1c} = F(\Pi_c - \Pi)^\beta$, where $x_1^{(a)}$ and $x_1^{(b)}$ are the mole fraction of DChol in the two coexisting phases, the mole fraction of DChol of the critical mixture $x_{1c} = 0.26$, the critical pressure $\Pi_c = 10.2 \text{ mN/m}$, and the adjustable parameter $F = 1.1282$. The rectilinear rule is used in sketching the rest of the curve (King, 1969).

the phase contrast. A glass capillary insulated tungsten wire ($6 \mu\text{m}$ in diameter) with a total diameter of $\sim 20 \mu\text{m}$ poked through the monolayer from the subphase and acted as an electrode. An electrical potential V_0 was applied between the electrode and the subphase, establishing an inhomogeneous electric field $\mathcal{E}(r)$ at the air–water interface. A molecule in the monolayer at a distance r away from the electrode feels a force proportional to its dipole moment and the field gradient $\partial\mathcal{E}/\partial r$. Whether the force is attractive or repulsive depends on the polarity of V_0 and the dipole orientation (Klingler and McConnell, 1993). All experiments were performed at room temperature and at various surface pressures. (See Fig. 2.)

When the monolayer has a composition in the two-phase coexistence region and is held at a surface pressure well below the mixing–demixing line, it consists of small domains of dark DChol-rich phase, interspersed uniformly through a bright DMPC-rich phase, or vice versa. Application of a negative potential to the electrode leads to the attraction and fusion of dark domains around the electrode (Heckl et al., 1988; Klingler and McConnell, 1993; Lee and McConnell, 1993). The fused domain grows in size as a function of time until a steady state is reached where the attraction experienced by the small domains from the applied field is balanced by the repulsion from the large fused domain (see Fig. 3 a).

For a surface pressure and composition such that the monolayer is in the single-phase region above the mixing–demixing line but below the critical pressure, the film is homogeneous in the fluorescence microscope. Application of a negative potential to the electrode leads to the formation of a dark domain with a sharp edge around

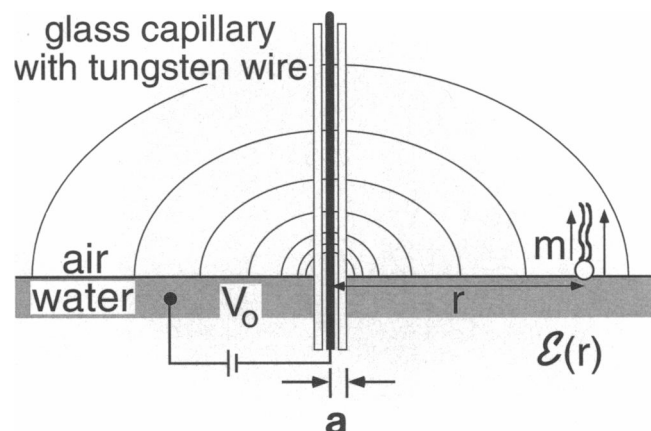


FIGURE 2 Schematic for the setup of an inhomogeneous electric field at the air–water interface. An electric potential V_0 is applied to an insulated tungsten wire, creating an inhomogeneous electric field $\mathcal{E}(r)$ at the air–water interface that exerts a force on molecular dipoles. The radius of the insulated electrode is a , which is $\sim 6 \mu\text{m}$.

the electrode. The dark domain grows in size until equilibrium is reached (see Fig. 3 b). This large dark domain is not formed by fusion of small domains, because they are not present in the homogeneous state. If the polarity of the potential is reversed quickly, the domain around the electrode “explodes,” forming little fragments with sharp edges (see Fig. 3 c). These fragments drift away from the electrode and disappear within 30 s. The monolayer reverts to its initial homogeneous state.

When the monolayer has a critical composition and is held just above the critical pressure, it is also homogeneous in the fluorescence microscope. Unlike in the previous case where phase separation with a sharp boundary is formed, the application of a negative potential to the electrode gives rise to a brightness gradient, from dark around the electrode, to bright at large distances (see Fig. 3 d). The concentration gradient is continuous and shows no distinct boundary. Upon rapid reversal of the potential, diffuse dark regions are expelled from the electrode (see Fig. 3 e) and quickly disappear. If the reversed polarity is sustained, a diffuse bright ring is formed around the electrode (see Fig. 3 f).

THERMODYNAMIC MODELS OF BINARY LIQUID MIXTURES

We model the effect of an externally applied inhomogeneous electric field on the monolayer by using equilibrium chemical thermodynamics. Four different cases are considered: (1) regular solutions with symmetric phase diagrams, (2) regular solutions with asymmetric phase diagrams, (3) nonideal mixing with symmetric phase diagrams, and (4) real solutions with asymmetric phase diagrams. Nonlocal chemical potentials due to internal electric fields within the monolayer are discussed later.

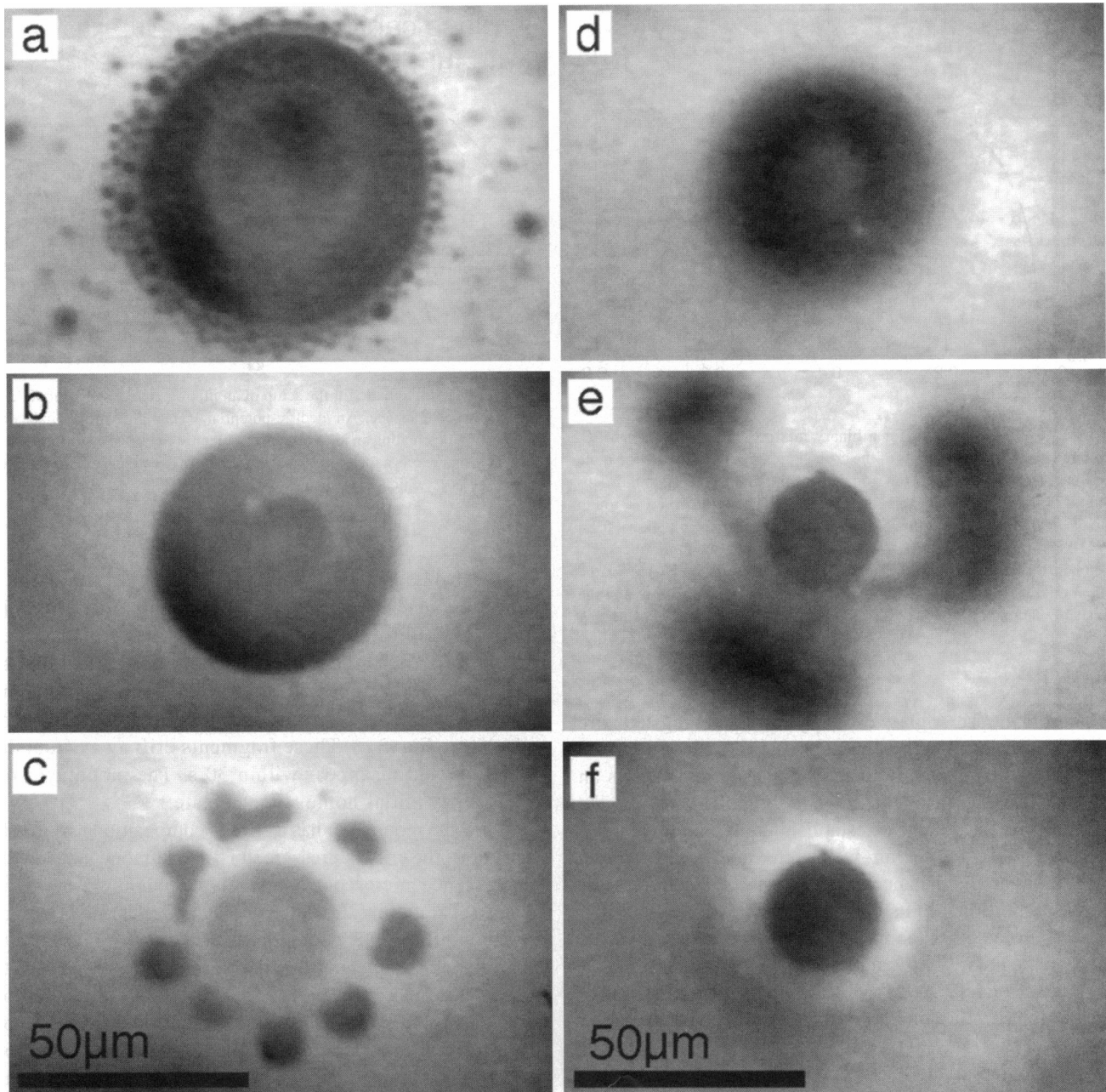


FIGURE 3 Fluorescence micrographs of DChol-DMPC monolayers in the presence of an inhomogeneous electric field. (a) Fusion of domains in the two-phase coexistence region with a negative potential ($V_0 = -13$ V) applied; $\Pi = 3.0$ mN/m. (b) Formation of a domain with a sharp edge for a system that is in the homogeneous region below the critical pressure in the absence of the field. A negative potential ($V_0 = -100$ V) was applied; $\Pi = 8.6$ mN/m. (c) Same experiment as in (b) 100 ms after reversing the potential to positive. The previously formed domain explodes into smaller fragments, which quickly disappear. (d) Steady-state concentration gradient formed above the critical pressure with a negative potential applied ($V_0 = -208$ V); $\Pi = 10.3$ mN/m. (e) Same experiment as in (d) 100 ms after reversing the potential to positive. Dark, diffuse regions are expelled from the electrode. (f) Steady-state concentration gradient formed using a positive potential.

Case (1): Regular solution with symmetric phase diagrams

The simplest possible model is an ideal binary mixture whose phase diagram is symmetric about the critical composition of $x_{1c} = x_{2c} = 0.5$, where x_{1c} and x_{2c} are the critical mole fractions of components 1 and 2 (see Fig. 4 a). For this mixture,

the relative proportions of the two phases remain constant as the temperature T is increased toward the critical temperature T_c , at which point the two phases merge to form a homogeneous single phase. In the case of experiments where temperature is held constant at room temperature and surface pressure Π is varied, the homogeneous phase is found when the critical surface pressure Π_c is reached.

Composition gradients of the two components are set up around the electrode in Fig. 2. The mole fractions x_1 and x_2 become functions of position r . Incorporating the contribution of the electric field $\mathcal{E}(r)$, the chemical potentials of the two components, μ_1 and μ_2 , are assumed to be (Kirkwood and Oppenheim, 1961)

$$\begin{aligned} \mu_1(\Pi + \pi) &= \mu_1^{(0)}(\Pi) + RT \ln x_1 + \bar{A}_1 \pi + \alpha x_2^2 - m_1 \bar{A}_1 \mathcal{E}(r), \quad (1) \\ &= \mu_1^{(0)}(\Pi) + RT \ln x_1 + \bar{A}_1 \pi + \alpha x_2^2 - m_1 \bar{A}_1 \mathcal{E}(r), \end{aligned}$$

$$\begin{aligned} \mu_2(\Pi + \pi) &= \mu_2^{(0)}(\Pi) + RT \ln x_2 + \bar{A}_2 \pi + \alpha x_1^2 - m_2 \bar{A}_2 \mathcal{E}(r), \quad (2) \\ &= \mu_2^{(0)}(\Pi) + RT \ln x_2 + \bar{A}_2 \pi + \alpha x_1^2 - m_2 \bar{A}_2 \mathcal{E}(r), \end{aligned}$$

where $\mu_1^{(0)}(\Pi)$ and $\mu_2^{(0)}(\Pi)$ are the chemical potentials of pure liquids 1 and 2, respectively, R is the universal gas constant, T is the temperature, Π is the surface pressure of the system a large distance away from the electrode, π is the surface pressure change induced by the presence of the field and varies with distance from the electrode, and m_1 , m_2 and \bar{A}_1 , \bar{A}_2 are the dipole moment densities and partial molar areas of the two components, respectively. Here we use the sign convention of both positive \mathcal{E} and m pointing into the subphase. When $\mathcal{E} = \pi = 0$ the mixing-demixing parameter α is related to the critical temperature of the system by $\alpha = 2RT_c$.

The molar area of a binary mixture \bar{A} is related to the partial molar areas of its two constituents, \bar{A}_1 and \bar{A}_2 by

$$\bar{A} = x_1 \bar{A}_1 + x_2 \bar{A}_2. \quad (3)$$

In this ideal case there is neither contraction nor expansion upon mixing, and the resulting molar area $\bar{A}^{(0)} = x_1 \bar{A}_1^{(0)} + x_2 \bar{A}_2^{(0)}$; $\bar{A}_1^{(0)}$ and $\bar{A}_2^{(0)}$ are the molar areas of pure liquids 1 and 2. For the mixing of regular solutions, it can be assumed that the partial molar volume of each component is equal to that of its corresponding pure liquid ($\bar{A}_1 = \bar{A}_1^{(0)}$; $\bar{A}_2 = \bar{A}_2^{(0)}$); thus $\bar{A} = \bar{A}^{(0)}$ (Kirkwood and Oppenheim, 1961).

At equilibrium, the chemical potential gradients are zero:

$$\frac{\partial \mu_1}{\partial r} = \frac{RT}{x_1} \frac{\partial x_1}{\partial r} + \bar{A}_1^{(0)} \frac{\partial \pi}{\partial r} + 2\alpha x_2 \frac{\partial x_2}{\partial r} - m_1 \bar{A}_1^{(0)} \frac{\partial \mathcal{E}}{\partial r} = 0, \quad (4)$$

$$\frac{\partial \mu_2}{\partial r} = \frac{RT}{x_2} \frac{\partial x_2}{\partial r} + \bar{A}_2^{(0)} \frac{\partial \pi}{\partial r} + 2\alpha x_1 \frac{\partial x_1}{\partial r} - m_2 \bar{A}_2^{(0)} \frac{\partial \mathcal{E}}{\partial r} = 0. \quad (5)$$

Combining Eqs. 4 and 5, we see that the pressure gradient and the electric field gradient are related:

$$\bar{A}^{(0)} \frac{\partial \pi}{\partial r} = \bar{M}^{(0)} \frac{\partial \mathcal{E}}{\partial r}, \quad (6)$$

where $\bar{M}^{(0)} = x_1 m_1 \bar{A}_1^{(0)} + x_2 m_2 \bar{A}_2^{(0)}$ is the ideal case of the molar dipole moment of the binary mixture \bar{M} defined more generally as

$$\bar{M} = x_1 m_1 \bar{A}_1 + x_2 m_2 \bar{A}_2. \quad (7)$$

Substituting Eq. 7 into Eq. 4, we find

$$\frac{\partial x_1}{\partial r} = \frac{x_1 x_2 \bar{A}_1^{(0)} \bar{A}_2^{(0)} (m_1 - m_2)}{(x_1 \bar{A}_1^{(0)} + x_2 \bar{A}_2^{(0)}) (RT - 2\alpha x_1 x_2)} \frac{\partial \mathcal{E}}{\partial r}. \quad (8)$$

For the special case where the molar areas of the two components of the mixture are identical ($\bar{A}_1^{(0)} = \bar{A}_2^{(0)} = \bar{A}^{(0)}$), Eq. 8 can be solved by separation of variables, and the position-dependent composition is found to vary with the field as

$$\left[\ln\left(\frac{1-x_1}{x_1}\right) + \frac{4T_c}{T} x_1 \right]_0^r = -\frac{\bar{A}^{(0)}}{RT} (m_1 - m_2) \mathcal{E}(r), \quad (9)$$

where $[f(r)]_0^r = f(r) - f(\infty)$; $x_1(r)$ refers to the mole fraction of component 1 at a distance r from the electrode and $x_1(\infty)$ the composition at large distances away from the electrode.

Fig. 5 plots the solutions to Eq. 9 and shows how x_1 varies with field strength for different initial compositions. For example, when the system is at its critical composition and held

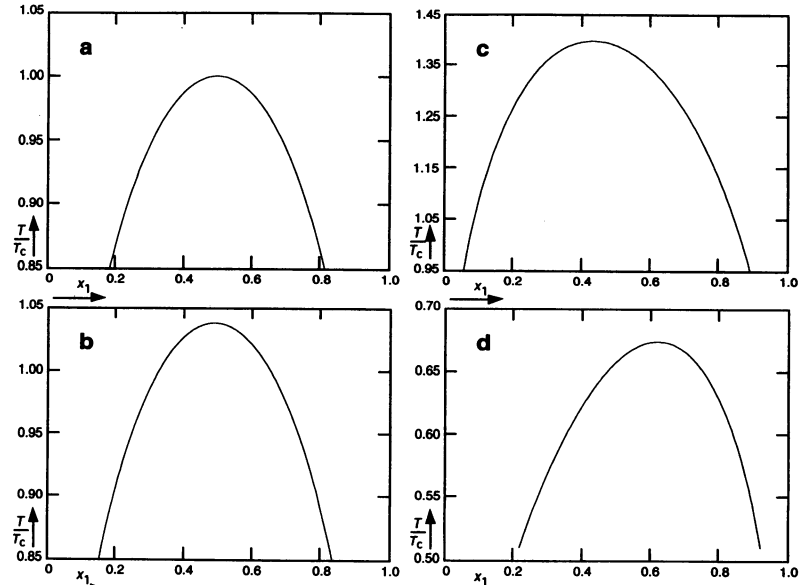


FIGURE 4 Reduced phase diagrams of T/T_c versus x_1 for various values of B_1 and C_1 . (a) $B_1 = \alpha$, $C_1 = 0$; (b) $B_1 = \alpha$, $C_1 = 0.1RT_c$; (c) $B_1 = \alpha$, $C_1 = RT_c$; (d) $B_1 = \alpha$, $C_1 = -RT_c$. Here T_c is the critical temperature of the symmetric regular solution system discussed in Case (1). See text.

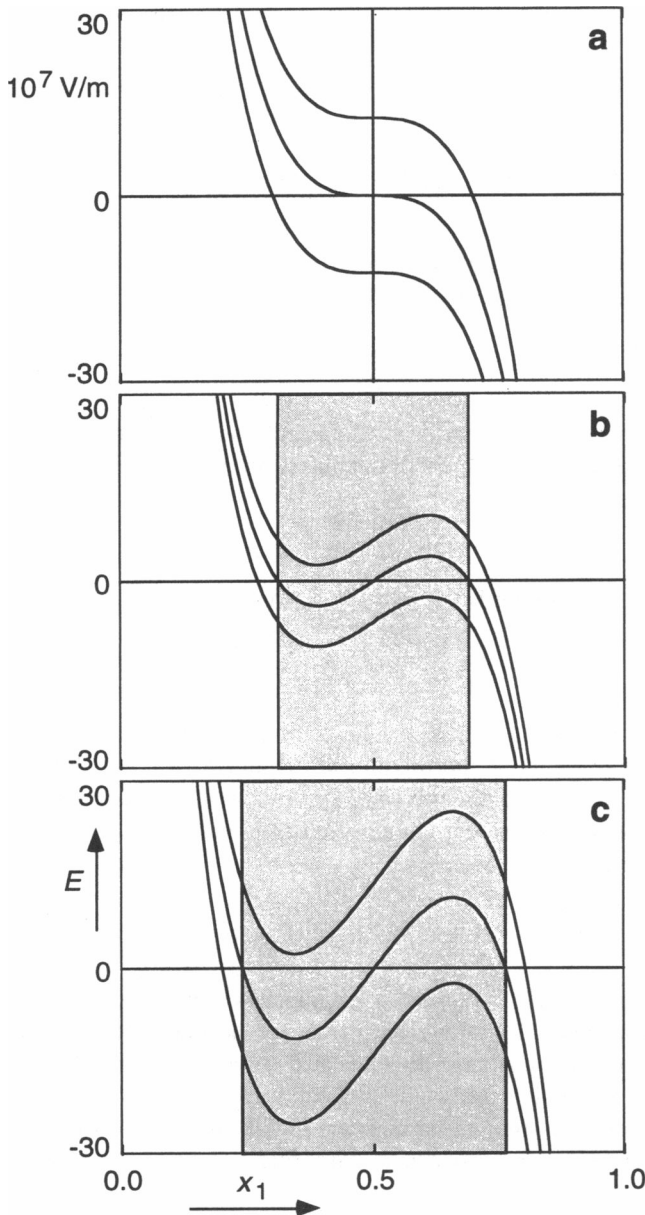


FIGURE 5 Composition variations for component 1 in a binary mixture of regular solutions with symmetric phase diagram (see Fig. 4 a) as a function of the electric field strength at various temperatures: (a) $T = 1.0T_c$, (b) $T = 0.95T_c$; (c) $T = 0.9T_c$. The shaded area denotes the two-phase coexistence region. Three curves are shown for each temperature. The middle curve has a composition corresponding to a point on the phase boundary in the absence of any external field, while the other two have initial compositions in the single-phase homogeneous regions that differ by the same amount on either side of the phase diagram. Parameters for model calculations: $T_c = 414 \text{ K}$, $m = -0.65 \text{ D/nm}^2$, $\bar{A} = \bar{A}_1 = \bar{A}_2 = 1 \text{ nm}^2/\text{molecule}$.

close to its critical temperature, $x_1(\infty) = 1/2$ and $T \approx T_c$ (see the middle curve in Fig. 5 a), a positive or negative electrode with a relatively low field strongly alters the concentration of component one around it. When $x_1(\infty)$ is outside the two-phase coexistence region to the left of the phase boundary for some $T < T_c$ (see the lower curve in Fig. 5 b or c), an increasing negative field (decreasing r for a negative electrode)

leads to a change in composition until the phase boundary is reached. At this point, field-induced phase separation occurs. For still smaller values of r only one phase is present. The composition of the phase surrounding the electrode then varies as indicated. Similar phase separations take place when a positive field is applied to a system with $x_1(\infty)$ outside the two-phase coexistence region to the right of the phase boundary (see the upper curve in Fig. 5 b or c). Note that the \mathcal{E} -versus- x_1 curves in the two-phase region describe metastable and unstable states where the maxima and minima define the spinodal.

Case (2): Regular solution with asymmetric phase diagrams

Now consider binary mixtures corresponding to regular solutions with asymmetric phase diagrams. In this case, the chemical potentials of components 1 and 2 are

$$\begin{aligned} \mu_1(\Pi + \pi) = & \mu_1^{(0)}(\Pi) + RT \ln x_1 \\ & + \bar{A}_1 \pi + B_1 x_2^2 + C_1 x_2^3 - m_1 \bar{A}_1 \mathcal{E}(r) + O(x_2^4), \end{aligned} \quad (10)$$

$$\begin{aligned} \mu_2(\Pi + \pi) = & \mu_2^{(0)}(\Pi) + RT \ln x_2 \\ & + \bar{A}_2 \pi + B_2 x_1^2 + C_2 x_1^3 - m_2 \bar{A}_2 \mathcal{E}(r) + O(x_1^4). \end{aligned} \quad (11)$$

Again we assume that $\bar{A}_1 = \bar{A}_1^{(0)}$ and $\bar{A}_2 = \bar{A}_2^{(0)}$ for regular solutions. It can be shown that in this case B_1 , B_2 , C_1 , and C_2 are constants not dependent on Π and that they are related to one another by $B_2 = B_1 + 1.5C_1$ and $C_2 = -C_1$ (Kirkwood and Oppenheim, 1961). Case (1) above is a special case of the present Case (2) where $B_1 = \alpha$ and $C_1 = 0$. The panels in Fig. 3 show how one can alter the shape of the phase diagram as well as the critical composition of the system by varying the values of B_1 and C_1 .

At equilibrium, the position-independent chemical potentials of the two components yield the following equations:

$$\begin{aligned} RT \frac{\partial x_1}{\partial r} + x_1 \bar{A}_1^{(0)} \frac{\partial \pi}{\partial r} + 2B_1 x_1 x_2 \frac{\partial x_2}{\partial r} \\ + 3C_1 x_1 x_2^2 \frac{\partial x_2}{\partial r} - m_1 x_1 \bar{A}_1^{(0)} \frac{\partial \mathcal{E}}{\partial r} = 0, \end{aligned} \quad (12)$$

$$\begin{aligned} RT \frac{\partial x_2}{\partial r} + x_2 \bar{A}_2^{(0)} \frac{\partial \pi}{\partial r} + (2B_1 + 3C_1)x_1 x_2 \frac{\partial x_1}{\partial r} \\ - 3C_1 x_1 x_2 \frac{\partial x_1}{\partial r} - m_2 x_2 \bar{A}_2^{(0)} \frac{\partial \mathcal{E}}{\partial r} = 0. \end{aligned} \quad (13)$$

The combination of Eqs. 12 and 13 gives a relation identical to that in Eq. 6. The composition gradients and the field gradient are related by

$$\frac{\partial x_1}{\partial r} = \frac{x_1 x_2 \bar{A}_1^{(0)} \bar{A}_2^{(0)} (m_1 - m_2)}{(x_1 \bar{A}_1^{(0)} + x_2 \bar{A}_2^{(0)}) (RT - 2B_1 x_1 x_2 - 3C_1 x_1 x_2^2)} \frac{\partial \mathcal{E}}{\partial r}, \quad (14)$$

$$\frac{\partial x_2}{\partial r} = \frac{-x_1 x_2 \bar{A}_1^{(0)} \bar{A}_2^{(0)} (m_1 - m_2)}{(x_1 \bar{A}_1^{(0)} + x_2 \bar{A}_2^{(0)}) [RT - (2B_1 + 3C_1)x_1 x_2 + 3C_1 x_1^2 x_2]} \frac{\partial \mathcal{E}}{\partial r}. \quad (15)$$

For the special case of identical molar areas, the position-dependent compositions are

$$\left[\ln\left(\frac{1 - x_1}{x_1}\right) + \frac{2B_1 + 3C_1}{RT} x_1 - \frac{3}{2RT} C_1 x_1^2 \right]_{\infty}^r = -\frac{\bar{A}^{(0)}}{RT} (m_1 - m_2) \mathcal{E}(r), \quad (16)$$

$$\left[-\ln\left(\frac{1 - x_2}{x_2}\right) - \frac{2B_1}{RT} x_2 - \frac{3}{2RT} C_1 x_2^2 \right]_{\infty}^r = -\frac{\bar{A}^{(0)}}{RT} (m_1 - m_2) \mathcal{E}(r). \quad (17)$$

Equation 16 reduces to Eq. 9 when B_1 equals α and C_1 is zero.

The panels in Fig. 6 show how the different initial compositions at different temperatures change with field strength for a system where $B_1 = 2RT_c$ and $C_1 = RT_c$; T_c is the critical temperature for Case (1). The phase diagram of this system is shown in Fig. 4 c. Like the solutions to Eq. 9 in Fig. 5, the variations of composition show similar qualitative behavior in response to positive and negative electric fields for all temperatures at and below the critical temperature. Unlike in the former case, however, the shapes of the curves are no longer "symmetric" about midcomposition but vary with different values of B_1 and C_1 .

Case (3): Nonideal mixing with symmetric phase diagrams

Area expansion or contraction usually occurs upon mixing. Consider the case of nonideal mixing where the partial molar areas of the two components are given by

$$\bar{A}_1 = \bar{A}_1^{(0)} + \Delta x_1^2, \quad (18)$$

$$\bar{A}_2 = \bar{A}_2^{(0)} + \Delta x_2^2. \quad (19)$$

Here Δ is the expansion/contraction (positive/negative) parameter for mixing. When Eqs. 18 and 19 are substituted into 3, the molar area of the mixture is then

$$\bar{A} = x_1 \bar{A}_1^{(0)} + x_2 \bar{A}_2^{(0)} + \Delta x_1 x_2. \quad (20)$$

With a non-zero expansion/contraction parameter, the dipole moment densities m_1 and m_2 are no longer constants but vary with position r . We shall assume that the molar dipole densities $\bar{M}_1 = m_1 \bar{A}_1$ and $\bar{M}_2 = m_2 \bar{A}_2$ are constant. This is a physically plausible assumption for the coexisting liquid phases that we are considering but would certainly *not* be a plausible assumption for coexisting liquid and gas phases. For a gas phase the dipole density that appears in the theory is doubtless dominated by water molecules.

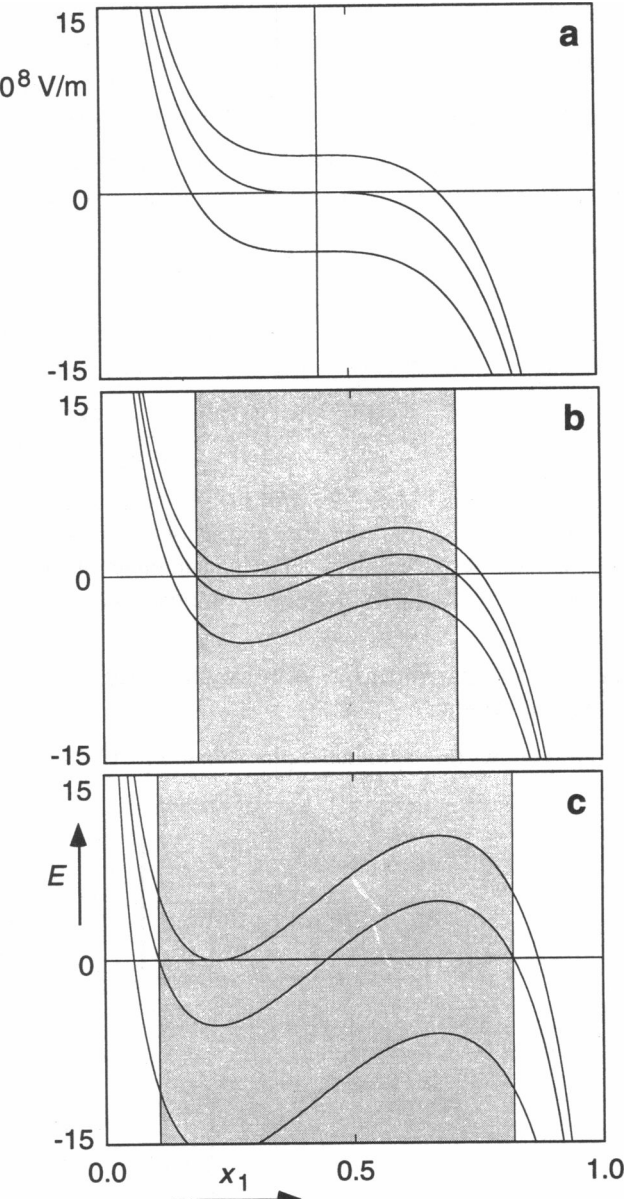


FIGURE 6 Composition variations for component 1 in a binary mixture of regular solutions with an asymmetric phase diagram (see Fig. 4 c) as a function of the electric field strength at various temperatures: (a) $T = 1.1T_c$; (b) $T = 1.25T_c$; (c) $T = 1.395T_c$. The mixing-demixing parameters are given by $B_1 = 2RT_c$ and $C_1 = RT_c$. The middle curve has a composition corresponding to a point on the phase boundary in the absence of any external field, while the other two have initial compositions in the single-phase homogeneous regions that differ by the same amount on either side of the phase diagram. Parameters for model calculations: $T_c = 414$ K, $m = -0.65$ D/nm², $\bar{A} = \bar{A}_1 = \bar{A}_2 = 1$ nm²/molecule.

To study the effect of area expansion or contraction on the composition gradient in the presence of electric field, we return to a model similar to that of Case (1), where the phase diagram of the binary mixture is symmetric but the mixing is nonideal. When we use Eqs. 18 and 19, the chemical potentials are then given by

$$\mu_1(\Pi + \pi) \quad (21)$$

$$\begin{aligned}
&= \mu_1^{(0)}(\Pi) + RT \ln x_1 + \bar{A}_1^{(0)}\pi + (\alpha + \Delta\pi)x_2^2 - \bar{M}_1\mathcal{E}(r), \\
\mu_2(\Pi + \pi) &= \mu_2^{(0)}(\Pi) + RT \ln x_2 + \bar{A}_2^{(0)}\pi + (\alpha + \Delta\pi)x_1^2 - \bar{M}_2\mathcal{E}(r).
\end{aligned} \tag{22}$$

Carrying out the same analysis as before, we find that the surface pressure gradient and the field gradient are related by

$$\frac{\partial\pi}{\partial r} = \frac{\bar{M}}{\bar{A}} \frac{\partial\mathcal{E}}{\partial r}, \tag{23}$$

where $\bar{M} = x_1\bar{M}_1 + x_2\bar{M}_2$ and \bar{A} is given by Eq. 20. The composition gradient is then related to the field gradient by

$$\frac{\partial x_1}{\partial r} = \frac{x_1x_2(\bar{A}_2\bar{M}_1 - \bar{A}_1\bar{M}_2)}{(x_1\bar{A}_1 + x_2\bar{A}_2)[RT - 2(\alpha + \Delta\pi)x_1x_2]} \frac{\partial\mathcal{E}}{\partial r}. \tag{24}$$

Comparing Eqs. 21 and 22 with Eqs. 1 and 2, and Eq. 24 with Eq. 8, we see that the area expansion/contraction parameter modifies the mixing–demixing parameter of the system, making it explicitly dependent on pressure.

Case (4): Real solutions with asymmetric phase diagrams

Figure 1 shows the asymmetric phase diagram of DChol and

$$\begin{aligned}
\frac{\partial x_1}{\partial r} &= \frac{1}{RT - 2B_1x_1x_2 - 3C_1x_1x_2^2} \left[x_1\bar{M}_1 - \frac{(x_1\bar{M}_1 + x_2\bar{M}_2)\left(\frac{\partial B_1}{\partial\pi}x_1x_2^2 + \frac{\partial C_1}{\partial\pi}x_1x_2^3 + x_1\bar{A}_1^{(0)}\right)}{\frac{\partial B_1}{\partial\pi}x_1x_2 + \frac{\partial C_1}{\partial\pi}x_1x_2\left(1 - \frac{x_1}{2}\right) + x_1\bar{A}_1^{(0)} + x_2\bar{A}_2^{(0)}} \right] \frac{\partial\mathcal{E}}{\partial r}, \\
\frac{\partial x_2}{\partial r} &= \frac{1}{RT - (2B_1 + 3C_1)x_1x_2 + 3C_1x_1^2x_2} \\
&\quad \left\{ x_2\bar{M}_2 - \frac{(x_1\bar{M}_1 + x_2\bar{M}_2)\left[\left(\frac{\partial B_1}{\partial\pi} + \frac{3}{2}\frac{\partial C_1}{\partial\pi}\right)x_1^2x_2 - \frac{\partial C_1}{\partial\pi}x_1^3x_2 + x_2\bar{A}_2^{(0)}\right]}{\frac{\partial B_1}{\partial\pi}x_1x_2 + \frac{\partial C_1}{\partial\pi}x_1x_2\left(1 - \frac{x_1}{2}\right) + x_1\bar{A}_1^{(0)} + x_2\bar{A}_2^{(0)}} \right\} \frac{\partial\mathcal{E}}{\partial r}.
\end{aligned} \tag{30, 31}$$

DMPC. The work of Phillips gives area contraction for cholesterol and phospholipid upon mixing (Phillips, 1972). From the analysis in the previous case, we have shown that the area expansion/contraction parameter alters the mixing–demixing parameter of the system. Therefore, the simplest model for the monolayer has the chemical potentials

$$\begin{aligned}
\mu_1(\Pi + \pi) &= \mu_1^{(0)}(\Pi) + RT \ln x_1 + \bar{A}_1^{(0)}\pi + B_1(\Pi + \pi, T)x_2^2 \\
&\quad + C_1(\Pi + \pi, T)x_2^3 - \bar{M}_1\mathcal{E}(r) + \vartheta(x_2^4),
\end{aligned} \tag{25}$$

$$\begin{aligned}
\mu_2(\Pi + \pi) &= \mu_2^{(0)}(\Pi) + RT \ln x_2 + \bar{A}_2^{(0)}\pi + B_2(\Pi + \pi, T)x_1^2 \\
&\quad + C_2(\Pi + \pi, T)x_1^3 - \bar{M}_2\mathcal{E}(r) + \vartheta(x_1^4).
\end{aligned} \tag{26}$$

The coefficients B_1 , B_2 , C_1 , and C_2 , though still related by the equations shown in Case (2), are no longer constants

but are now functions of surface pressure, and the area expansion/contraction effect is now included in these coefficients.

The zero chemical potential gradients at equilibrium yield the relations

$$\begin{aligned}
RT \frac{\partial x_1}{\partial r} + x_1x_2^2 \frac{\partial B_1}{\partial\pi} \frac{\partial\pi}{\partial r} + 2B_1x_1x_2 \frac{\partial x_2}{\partial r} + x_1x_2^3 \frac{\partial C_1}{\partial\pi} \frac{\partial\pi}{\partial r} \\
+ 3C_1x_1x_2^2 \frac{\partial x_2}{\partial r} + x_1\bar{A}_1^{(0)} \frac{\partial\pi}{\partial r} - x_1\bar{M}_1 \frac{\partial\mathcal{E}}{\partial r} = 0,
\end{aligned} \tag{27}$$

$$\begin{aligned}
RT \frac{\partial x_2}{\partial r} + x_1^2x_2 \left(\frac{\partial B_1}{\partial\pi} + \frac{3}{2} \frac{\partial C_1}{\partial\pi} \right) \frac{\partial\pi}{\partial r} \\
+ (2B_1 + 3C_1)x_1x_2 \frac{\partial x_1}{\partial r} - x_1^3x_2 \frac{\partial C_1}{\partial\pi} \frac{\partial\pi}{\partial r} \\
- 3C_1x_1^2x_2 \frac{\partial x_1}{\partial r} + x_2\bar{A}_2^{(0)} \frac{\partial\pi}{\partial r} - x_2\bar{M}_2 \frac{\partial\mathcal{E}}{\partial r} = 0.
\end{aligned} \tag{28}$$

The sum of the two gives

$$\left[x_1x_2 \frac{\partial B_1}{\partial\pi} + x_1x_2 \left(1 - \frac{x_1}{2} \right) \frac{\partial C_1}{\partial\pi} + \bar{A}^{(0)} \right] \frac{\partial\pi}{\partial r} = \bar{M} \frac{\partial\mathcal{E}}{\partial r}. \tag{29}$$

The composition gradients for the two components are

If there is no contraction upon mixing, which corresponds to constant B_1 , C_1 , m_1 , m_2 , Eqs. 30 and 31 reduce to Eqs. 14 and 15 as in Case (2). This in turn leads to the solutions given in Eqs. 16 and 17 for the special case of equal molar areas. Equations 30 and 31 as they stand cannot be solved analytically.

DISCUSSION

Comparison with experimental results

An important quantitative experimental result is that for the case of field-induced phase separation, the domain gathered around the electrode reaches an equilibrium size with a given potential (see Figs. 3 b and 7). The edge of the domain signifies the location where the local composition matches that at the two-phase coexistence boundary. In the analysis of Cases (1) and (2) where there is no area contraction, the composition at the phase boundary is independent on the

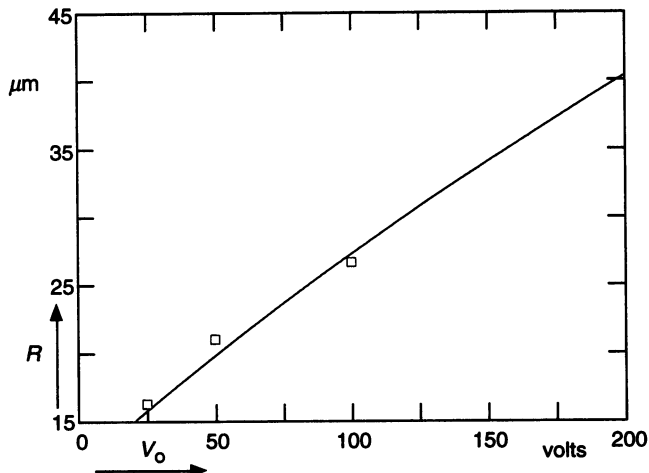


FIGURE 7 Equilibrium radii at the perimeter of field-induced domains versus applied potential: experimental results (\square); theoretical calculations (—). Parameters for model calculations: $\Pi = 8.6 \text{ mN/m}$, $T = 295 \text{ K}$, $x_1(\infty) = 0.10035$, and x_1 (phase boundary) $|_{\pi=0} = 0.1006$.

applied field. The edge of the gathered domain therefore experiences a field given by the intersection of the sigmoid composition variation curve and the straight phase boundary line as shown in Figs. 5 b and c and 6 b and c. However, for the case of real solutions where the system contracts or expands upon mixing, the thermodynamic parameters are functions of surface pressure, which in turn changes with the applied field according to Eq. 29. In order to see how closely the model approximates our experimental results on equilibrium domain size, we solve Eqs. 29–31 numerically under the conditions given in the Experimental Results section. Approximate dipole moment densities and molar areas can be obtained from the literature (Benvegnu and McConnell, 1993; Phillips, 1972). The mixing parameters B_1 and C_1 , their variations with respect to surface pressure, and the variation of the electric field with distance are also necessary for these numerical calculations.

In the absence of the external electric field, the system has the phase diagram of Fig. 1. For a binary mixture in the two-phase coexistence region to be at equilibrium, the chemical potentials for each component in the two phases are equal:

$$\begin{aligned} RT \ln x_1^{(a)} + B_1 x_2^{(a)2} + C_1 x_2^{(a)3} \\ = RT \ln x_1^{(b)} + B_1 x_2^{(b)2} + C_1 x_2^{(b)3}, \end{aligned} \quad (32)$$

$$\begin{aligned} RT \ln x_2^{(a)} + \left(B_1 + \frac{3}{2} C_1 \right) x_1^{(a)2} - C_1 x_1^{(a)3} \\ = RT \ln x_2^{(b)} + \left(B_1 + \frac{3}{2} C_1 \right) x_1^{(b)2} - C_1 x_1^{(b)3}, \end{aligned} \quad (33)$$

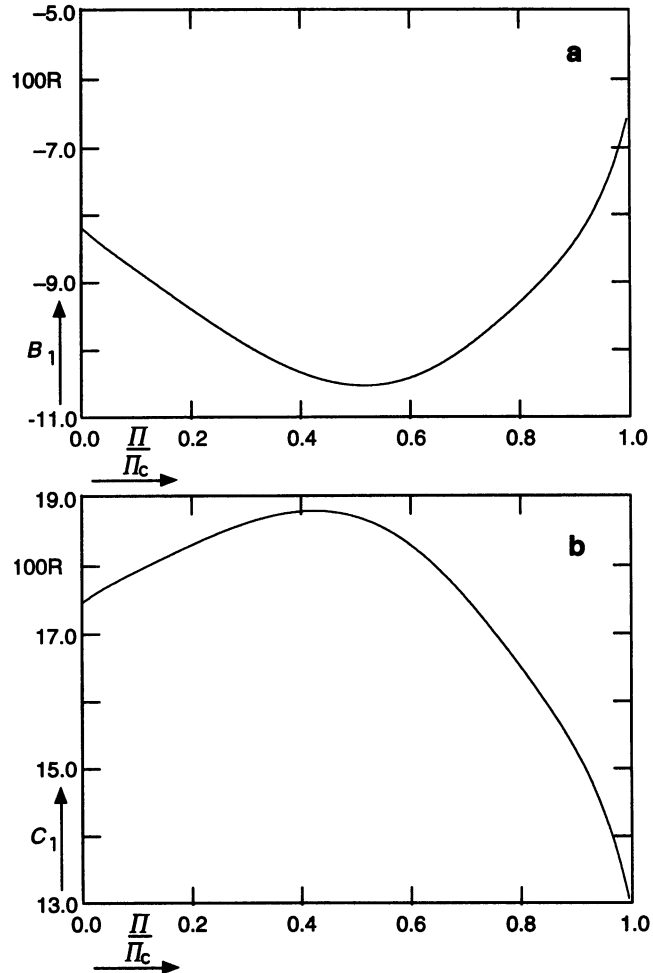


FIGURE 8 Surface pressure dependence of coefficients B_1 and C_1 obtained from solving Eqs. 34 and 35 for the phase diagram in Fig. 1. The vertical axis is expressed in units of $100 \times R$, where R is the universal gas constant (8.314 J/mol K).

where $x_i^{(j)}$ is the mole fraction of component i in phase j . With the knowledge of the compositions at both sides of the mixing–demixing curve for a given surface pressure, the coefficients B_1 and C_1 can be calculated by use of the following equations:

$$B_1 = \frac{RT(\ln x_1^{(a)} - \ln x_2^{(b)}) + (x_2^{(a)3} - x_2^{(b)3})C_1}{x_2^{(b)2} - x_2^{(a)2}}, \quad (34)$$

Using the phase diagram in Fig. 1, we have obtained values for the mixing–demixing parameters for different surface pressures. The surface pressure dependence of these two coefficients is shown in Fig. 8, from which $\partial B_1 / \partial \pi$ and $\partial C_1 / \partial \pi$ can be determined.

$$C_1 = \frac{RT \left[\ln x_2^{(b)} - \ln x_2^{(a)} + \frac{x_1^{(a)2} - x_1^{(b)2}}{x_2^{(b)2} - x_2^{(a)2}} (\ln x_1^{(b)} - \ln x_1^{(a)}) \right]}{\left[\frac{3}{2} (x_1^{(a)2} - x_1^{(b)2}) - x_1^{(a)3} + x_1^{(b)3} + \frac{(x_1^{(a)2} - x_1^{(b)2})(x_2^{(a)3} - x_2^{(b)3})}{x_2^{(b)2} - x_2^{(a)2}} \right]}. \quad (35)$$

Next we need to find the distance variation of the electric field. For the geometry depicted in Fig. 2 it has been shown that the electrode produces a field in the monolayer plane given by

$$\mathbf{E} = (0, 0, \mathcal{E}), \quad (36)$$

$$\mathcal{E}(r) = \frac{2V_0}{\pi} \int_0^\infty \frac{K_0(kr)}{K_0(ka)} dk, \quad (37)$$

where r is the distance from the center of the electrode, a is the radius of the electrode, V_0 is the potential applied, and K_0 is the zeroth-order modified Bessel function of the second kind. The electric field gradient is

$$\frac{\partial \mathcal{E}(r)}{\partial r} = -\frac{2V_0}{\pi r^2} \int_0^\infty \frac{u K_1(u)}{K_0\left(\frac{a}{r} u\right)} du, \quad (38)$$

where K_1 is the first-order modified Bessel function of the second kind. (Note that in Klingler and McConnell (1993) there is a typographical omission of a factor of u under the integral, which subsequently led to the erroneous conclusion in Lee et al. (1994) that the field-induced phase separated domains grow until the field gradient reaches a critical value. Our calculations show that the domains grow until a critical value for the field, *not* for the field gradient, is attained.)

Using the above information, we can numerically calculate the variation of electric field, surface pressure, local composition, and phase boundary with distance from the electrode for any given potential, initial surface pressure, and composition. The calculations have been carried out for $\Pi = 8.6 \text{ mN/m}$, $T = 295 \text{ K}$, $80 \text{ V} \leq V_0 \leq 200 \text{ V}$, $\bar{A}_1/N = 40 \text{ \AA}^2$, $\bar{A}_2/N = 80 \text{ \AA}^2$, where N is Avogadro's number. The initial composition, $x_1(\infty) = 0.10035$, is chosen so that it is close to one end of the phase boundary at zero field, which is at $x_1 = 0.1006$ under the above conditions.

At large distances away from the electrode, both the field and the field-induced pressure change are zero ($\mathcal{E} = \pi = 0$). As the distance from the electrode decreases, these values become nonzero and vary with distance r . At any given point r from the electrode, the electric field $\mathcal{E}(r)$ induces a surface pressure change $\pi(r)$ on the system. This in turn alters the phase boundary composition, rendering it position dependent. The dotted curve (a) in Fig. 9 shows how the composition at the phase boundary varies with distance.

The local composition of the binary mixture also varies with distance from the electrode when a potential is applied. At large distances, the system maintains its initial composition. As the electrode is approached, the local composition varies with the field, whose magnitude increases with decreasing distance from the electrode. The solid curve (b) in Fig. 9 shows how the local composition of component 1 varies with distance. As we move from infinity toward the electrode, the local composition passes through one point where the chemical potentials of the two components (Eqs. 25 and 26) in the two phases are simultaneously satisfied.

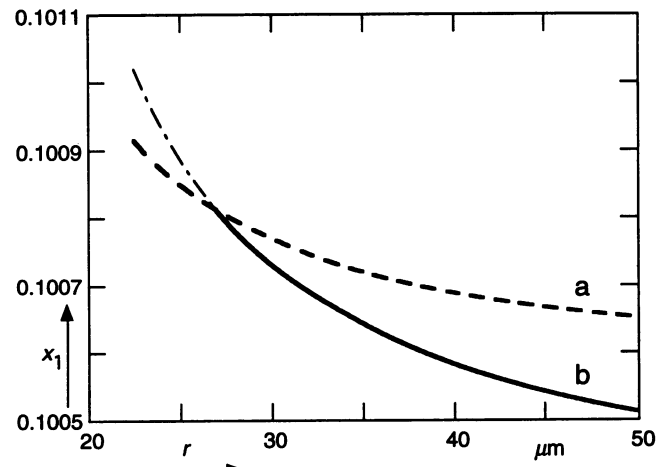


FIGURE 9 Distance variation of (a) the phase boundary composition (---) and (b) the local composition (—), calculated by solving Eqs. 29, 30, and 38. Parameters for model calculations: $\Pi = 8.6 \text{ mN/m}$, $T = 295 \text{ K}$, $V_0 = -100 \text{ V}$, $a = 10 \mu\text{m}$, $x_1(\infty) = 0.10035$, and x_1 (phase boundary) $|_{\mathcal{E}=0} = 0.1006$. The dotted-dashed portion of the local composition (---) signifies the metastable and spinodal part of the curve within the coexistence region.

This point is the intersection point between the local composition line and the phase boundary line as shown in Fig. 9. The dotted portion of the local composition signifies the metastable and spinodal part of the coexistence region. The intersection point also marks the location of the domain edge: for distances larger than that corresponding to the intersection point, no phase separation should occur. The calculated equilibrium domain sizes for different potentials are plotted in Fig. 7 along with experimental data for comparison. It can be seen that the theoretical work models experimental results semiquantitatively. The close quantitative correspondence between theory and experiment is due to the ad hoc choice of the initial composition x_1 .

Area expansion or contraction upon mixing

In the section on Case (4), we noted that area expansion or contraction occurs upon mixing together real solutions. Information regarding this change in area is embedded in the phase diagram of the system and can be extracted from it. The total area after mixing is

$$\bar{A} = x_1 \frac{\partial \mu_1}{\partial \pi} + x_2 \frac{\partial \mu_2}{\partial \pi}. \quad (39)$$

Using Eqs. 25 and 26, we find that

$$\begin{aligned} \bar{A} = & x_1 \left(\frac{\partial B_1}{\partial \pi} x_2^2 + \frac{\partial C_1}{\partial \pi} x_2^3 + \bar{A}_1^{(0)} \right) \\ & + x_2 \left[\left(\frac{\partial B_1}{\partial \pi} + \frac{3}{2} \frac{\partial C_1}{\partial \pi} \right) x_1^2 - \frac{\partial C_1}{\partial \pi} x_1^3 + \bar{A}_2^{(0)} \right]. \end{aligned} \quad (40)$$

Fig. 10 shows the area deviation from ideality when different compositions of DChol and DMPC are mixed at various pressures. The curves at low surface pressures agree

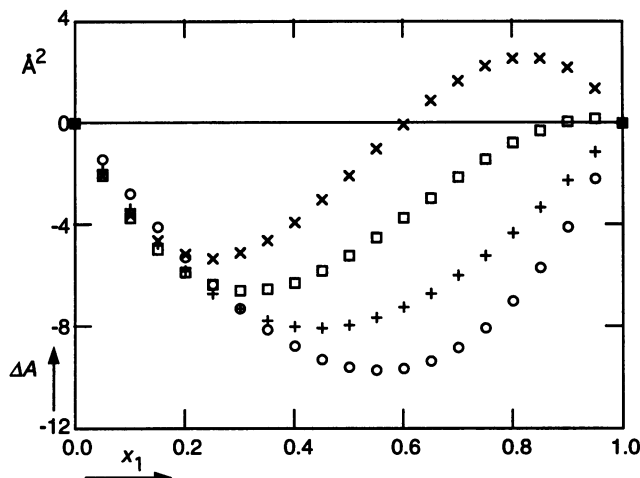


FIGURE 10 Area deviation from ideality at $\Pi/\Pi_c = 0.3$ (\circ); $\Pi/\Pi_c = 0.5$ (+); $\Pi/\Pi_c = 0.65$ (\square); $\Pi/\Pi_c = 0.843$ (\times).

semiquantitatively with those of Phillips (1972). At higher pressures, the curves show both contraction and expansion at different compositions. It should be noted that the results obtained here is sensitive to the phase boundary (see Eqs. 34, 35, and 40) of the diagram shown in Fig. 1, which is fit to an ad hoc curve. Any deviation of the fitted phase boundary from the true curve can affect the area contraction or expansion both quantitatively and qualitatively.

Contribution from electrostatic self energy

In previous sections, the only electrostatic energy explicitly incorporated in the model is due to the externally applied field. However, there are other contributions, namely, the electrostatic self-energy of the domain (McConnell and Moy, 1988). There are three electrostatic self-energy contributions. One is proportional to the domain area, one is proportional to the domain perimeter, and the third has the form of the self-induction energy of a current loop. The first term is the largest and is implicitly incorporated in the chemical potentials we have used and need not be considered further. The second term contributed to the interdomain line tension, and the third term is discussed further below.

As noted earlier, because of the dipole density difference between the two components in the binary mixture the application of an electric field leads to the attraction or repulsion of one component over the other. When the temperature (or surface pressure) is below its critical value, one of the two phases is preferentially attracted and fused around the electrode (see Fig. 3 *a* and *b*); Fig. 11 *a* shows schematically a single circular torus domain *A* with radii r_i , r_o and area A_A gathered around the electrode *W*. The electrostatic self-energy of the torus E_A is given by the expression

$$E_A = \epsilon_A A_A - \frac{m_A^2}{2} \int \int \frac{1}{\rho^3} dA_A dA_B, \quad (41)$$

where ϵ_A is the electrostatic energy per unit area for a domain

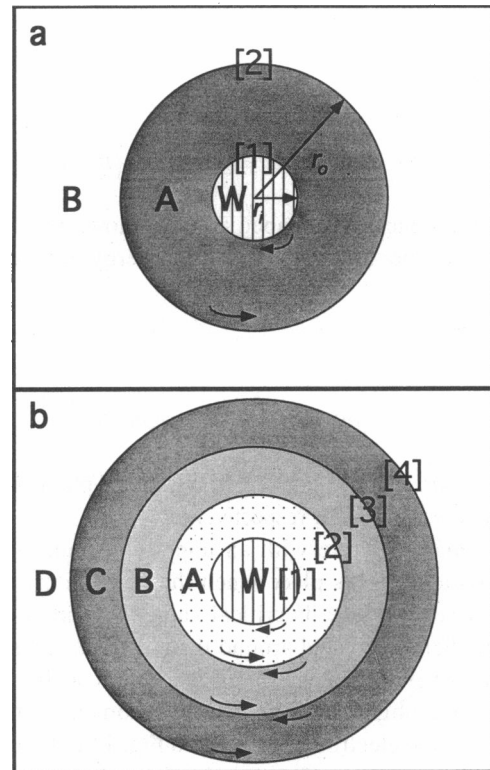


FIGURE 11 Schematics of (a) a single domain with a sharp edge gathered around the electrode, (b) a set of "infinite" torus shells, each with constant dipole moment density, depicting a concentration gradient set up around the electrode.

of infinite size with dipole density m_A , $\rho = (|\mathbf{r}_a - \mathbf{r}_b|^2 + \Delta_c^2)^{1/2}$ is the distance between two points of integration, *a* and *b*, and Δ_c is a cutoff that prevents the dipolar interaction from diverging when $|\mathbf{r}_a - \mathbf{r}_b| = 0$. The area integral gives the dipole repulsion between all dipoles within the area A_A and all dipoles exterior to it in area A_B .

This constitutes the shape-dependent portion of the electrostatic self-energy of domain *A*, which we denote as E_A^{sd} . This area integral can be expressed as a double line integral plus a correction term that equals the perimeter of the domain (McConnell and de Koker, 1992):

$$\int \int \frac{1}{\rho^3} dA_A dA_B = - \oint_A \oint_B \frac{1}{\rho} d\mathbf{r}_A \cdot d\mathbf{r}_B + 2P_{AA}, \quad (42)$$

where P_{AA} represents the perimeter of domain *A*. In the case of the torus in Fig. 11 *a*, this includes both the inner (P_{11}) and the outer (P_{22}) perimeters of the domain. Inasmuch as the outer perimeter of *B* extends to infinity, the line integral around it can be neglected because $1/\rho \rightarrow 0$. Using the convention that the material to be integrated lies to the left of the direction of the line integration, the line integrals over the inner perimeter of *B* and the outer perimeter of *A* are in opposite directions (Kaplan, 1984). However, because they overlap on the same path [2], it is convenient to let them be in the same direction. Denoting $\oint_i \oint_j (1/\rho) d\mathbf{r}_i d\mathbf{r}_j$ over the integral paths *i* and *j* (which both point in the same direction)

by $|ij|$, we can express E_A^{sd} as

$$E_A^{\text{sd}} = -\frac{m_A^2}{2} (|11| - |12| - |21| + |22|) - m_A^2(P_{11} + P_{22}). \quad (43)$$

For the circular torus-shaped domain shown in Fig. 11 *a*, the shape-dependent electrostatic self energy is found to be

$$E_A^{\text{sd}} = -2\pi m_A^2(r_i + r_o) + \frac{8\pi m_A^2(r_i r_o)^{1/2}}{k} [(1 - 0.5k^2)K - E] + 2\pi r_i m_A^2 \ln\left(\frac{e^2 \Delta}{8r_i}\right) + 2\pi r_o m_A^2 \ln\left(\frac{e^2 \Delta}{8r_o}\right), \quad (44)$$

where $k^2 = 4r_i r_o / (r_i + r_o)^2$ and K and E are elliptic integrals of the first and second kind, respectively.

For a binary mixture with an upper consolute point, no phase separation takes place when the temperature (or surface pressure) is above its critical value. Instead, a concentration gradient is created around the electrode. This can be modeled by having concentric circular torus shells, each of a constant but slightly different dipole moment density, radiating from the electrode as shown in Fig. 11 *b*. In this case, the total electrostatic self-energy includes the contributions from the individual tori as well as from the interaction energies among them. To simplify, consider a system with only torus-shaped domains A, B, and C. The electrostatic self-energy E_{ABC} of this system is

$$E_{ABC} = \epsilon_A A_A + \epsilon_B A_B + \epsilon_C A_C - \frac{m_A^2}{2} (|11| - |12| - |21| + |22|) - \frac{m_B^2}{2} (|22| - |23| - |32| + |33|) - \frac{m_C^2}{2} (|33| - |34| - |43| + |44|) + m_A m_B (-|12| + |13| + |22| - |23|) + m_A m_C (-|13| + |14| + |23| - |24|) + m_B m_C (-|23| + |24| + |33| - |34|) - m_A^2 P_{11} - m_C^2 P_{44} - (m_A^2 + m_B^2 - 2m_A m_B) P_{22} - (m_B^2 + m_C^2 - 2m_B m_C) P_{33}. \quad (45)$$

Equation 45 can be extended for systems with any arbitrary number of torus shells.

To see how significant this contribution is compared with that of the applied electric field, we carried out calculations for both the single-torus case and the case of "infinite" torus shells. For the single-torus case, we let the radius of the electrode $r_i = 10 \mu\text{m}$ and allow the domain (DChol) to grow to a radius $r_o = 50 \mu\text{m}$. We estimate m to be of the order of -1 D/nm^2 (Benvegnù and McConnell, 1993) and the applied electric field to be $\mathcal{E}(r) \geq (2/\pi) \cdot (V_0/r)$ for the geometry shown in Fig. 4 and for the size given above. From Eq. 44, we find that the self-energy

contribution $E_A^{\text{sd}} = -4.3 \times 10^{-16} \text{ J}$, which is small compared with that of the applied field

$$E_A^{\text{af}} \geq - \int_{r_i}^{r_o} m_A \frac{2}{\pi} \frac{V_0}{r} 2\pi r dr \sim -5.3 \times 10^{-14} \text{ J}$$

obtained by using a nominal applied voltage of $V_0 = -100 \text{ V}$.

The conclusion that these local electrostatic fields are negligible in our experiments can also be seen by simply comparing the applied field strength $\sim (2/\pi)(V_0/r)$ with the electric field at the edge of a single domain, when the dipole density difference is m . The latter is $(m/R_d) \ln(8R_d/e\Delta)$ when R_d is the domain radius (H. M. McConnell, unpublished calculations). For m of the order of -1 D/nm^2 , $R_d \geq 10 \mu\text{m}$, and $\Delta \sim 10 \text{ \AA}$, we see that an applied voltage of $10-100 \text{ V}$ will produce a much larger field intensity at the edge of a domain for any domain with a radius of experimental interest, $10-100 \mu\text{m}$.

For the case of the "infinite" torus shells, we set up a dipole density gradient for the critical composition ($x_1 = 0.26$; $x_2 = 0.74$), using the knowledge of the dipole densities of the two components, the $1/r$ falloff of the electric field, and the fact that the monolayer is at its critical composition at distances far away from the electrode. For shells extending from 10 to $100 \mu\text{m}$, each of $1-\mu\text{m}$ thickness, and each having its own constant dipole density obtained by averaging over the strip, we find the electrostatic self energy to be $-1.6 \times 10^{-15} \text{ J}$, which is 2 orders of magnitudes smaller than that of the applied field. From the above results, we can see that the omission of this special self-energy contribution in our equilibrium chemical potential calculations is justifiable.

Uniform Fields

For comparison, we briefly consider the effects of uniform electric fields on the phase behavior of monolayer membranes. First, consider a monolayer of one chemical component and two phases that are in equilibrium at temperature T and pressure Π . When a uniform field of strength \mathcal{E} is applied and the temperature is kept constant, the pressure changes from Π to $\Pi + \pi$. The surface pressure change can be expressed as

$$\pi = \frac{(\bar{M}_1 - \bar{M}_2)\mathcal{E}}{\bar{A}_1 - \bar{A}_2}, \quad (46)$$

where \bar{M}_1 and \bar{M}_2 are the molar dipole moments in phases 1 and 2, respectively, and \bar{A}_1 and \bar{A}_2 are the molar areas. Barring accidental cancellations, for $\mathcal{E} \sim -10^7 \text{ V/m}$, $(\bar{M}_1 - \bar{M}_2)/N \sim -1 \text{ D/molecule}$, and $(\bar{A}_1 - \bar{A}_2)/N \sim 50 \text{ \AA}^2$, where N is the Avogadro number, we obtain $\pi \sim 0.067 \text{ mN/m}$. This is far too small to affect significantly the monolayers studied under the usual conditions.

If the pressure is kept constant and the temperature is changed from T to $T + t$ to maintain equilibrium in the pres-

ence of an applied field of strength E , then

$$t = -\frac{T(\bar{M}_1 - \bar{M}_2)\mathcal{E}}{\bar{H}_1 - \bar{H}_2}, \quad (47)$$

where \bar{H}_1 and \bar{H}_2 are the molar enthalpy of the two phases. For $\bar{H}_1 - \bar{H}_2 \sim 2.6 \times 10^4 \text{ J/mol}$, we obtain $t \sim 10^{-4} \text{ deg}$, again a negligible change under most experimental conditions.

For a two-phase system corresponding to Case (1) above, a uniform field again yields the pressure change given in Eq. 46. If there is an area contraction as in Case (4), this pressure change will yield a change of critical temperature of the order of $\Delta\pi/2R, \sim 10^{-3} \text{ deg}$, again negligible for most experimental conditions.

Biological Membranes

The fundamental scaffolding of most biological membranes is the lipid bilayer. There is some evidence that, at the growth temperature, both prokaryotic and eukaryotic cell membranes are close to phase boundaries corresponding to lipid phase separations (Behan-Martin et al., 1993; Linden and Fox, 1975; Linden et al., 1973). One may consider the questions as to whether nonuniform electric fields exist in biological membranes and whether such fields can give rise to concentration gradients (or phase separations) of the sort discussed above.

Both the sign and the magnitude of the dipole densities in lipid monolayers are the same as those expected from the terminal methyl groups of lipids (Vogel and Möbius, 1988). Thus, it is plausible to assume that nonuniform fields acting in the center of the bilayers can give rise to composition gradients of lipid molecules. Such nonuniform fields could arise from point charges within a bilayer where electrostatic screening is weak. For example, a single electronic charge in a bilayer produces a field of the order of $1.44 \times 10^7 \text{ V/m}$ at a distance of 100 \AA . From our earlier discussion, this field strength is certainly adequate to yield a microscopic phase separation around the point charge, involving on the order of 100 molecules.

Externally applied fields that give rise to nonuniform transmembrane potentials may also produce significant lipid concentration gradients in biological membranes. These concentration gradients may be particularly large if, as we suspect, biological membranes under physiological growth conditions maintain their lipid compositions so as to be close to phase boundaries. Field-induced phase separations might well produce functional responses if they lead to receptor aggregation, for example.

We thank J. P. Hagen for his unpublished results on the phase diagram of DChol and DMPC. K. Y. C. L. is grateful for the National Research Service Award granted by the National Institutes of Health (grant 5T32 AI 07290-09). This work was supported by the National Science Foundation (grant NSF MCB 9316256).

REFERENCES

- Behan-Martin, M. K., G. R. Jones, K. Bowler, and A. R. Cossins. 1993. A near perfect temperature adaptation of bilayer order in vertebrate brain membranes. *Biochim. Biophys. Acta.* 1151:216–222.
- Benvegnu, D. J., and H. M. McConnell. 1993. Surface dipole densities in lipid monolayers. *J. Phys. Chem.* 97:6686–6691.
- Heckl, W. M., A. Miller, and H. Möhwald. 1988. Electric-field-induced domain movement in phospholipid monolayers. *Thin Solid Films.* 159: 125–132.
- Hirshfeld, C. L., and M. Seul. 1990. Critical mixing in monomolecular films: pressure-composition phase diagram of a two-dimensional binary mixture. *J. Phys. (Paris).* 51:1537–1552.
- Kaplan, W. 1984. Advanced Calculus. Addison-Wesley, Menlo Park, CA.
- King, M. B. 1969. Phase Equilibrium in Mixtures. Pergamon Press, Oxford.
- Kirkwood, J. G., and I. Oppenheim. 1961. Chemical Thermodynamics. McGraw-Hill, New York.
- Klingler, J. F., and H. M. McConnell. 1993. Field-gradient electrophoresis of lipid domains. *J. Phys. Chem.* 97:2962–2966.
- Knobler, C. M., and R. C. Desai. 1992. Phase transitions in monolayers. *Annu. Rev. Phys. Chem.* 43:207–236.
- Lee, K. Y. C., J. F. Klingler, and H. M. McConnell. 1994. Electric field induced concentration gradients in lipid monolayer. *Science.* 263:655–658.
- Lee, K. Y. C., and H. M. McConnell. 1993. Quantized shape transitions in lipid monolayer domains. *J. Phys. Chem.* 97:9532–9539.
- Linden, C. D., and C. F. Fox. 1975. Membrane physical state and function. *Acct. Chem. Res.* 8:321–327.
- Linden, C. D., K. L. Wright, H. M. McConnell, and C. F. Fox. 1973. Lateral phase separation in membrane lipids and the mechanism of sugar transport in *Escherichia coli*. *Proc. Natl. Acad. Sci. USA.* 70:2271–2275.
- McConnell, H. M. 1991. Structures and transitions in lipid monolayers at the air-water interface. *Annu. Rev. Phys. Chem.* 42:171–195.
- McConnell, H. M., and R. de Koker. 1992. Note on the theory of the sizes and shapes of lipid domains in monolayers. *J. Phys. Chem.* 96:7101–7103.
- McConnell, H. M., and V. T. Moy. 1988. Shapes of finite two-dimensional lipid domains. *J. Phys. Chem.* 92:4520–4525.
- Möhwald, H. 1990. Phospholipid and phospholipid-protein monolayers at the air/water interface. *Annu. Rev. Phys. Chem.* 41:441–476.
- Middleton, S. R., and B. A. Pethica. 1981. *Faraday Symp. Chem. Soc.* 16:109–123.
- Phillips, M. C. 1972. The physical state of phospholipids and cholesterol in monolayers, bilayers, and membrane. In *Progress in Surface and Membrane Science*. Vol. 5. Academic Press, New York. 139–221.
- Recktenwald, D. J., and H. M. McConnell. 1981. Phase equilibria in binary mixtures of phosphatidylcholine and cholesterol. *Biochemistry.* 20:4505–4510.
- Rice, P. A., and H. M. McConnell. 1989. Critical shape transitions of monolayer lipid domains. *Proc. Natl. Acad. Sci. USA.* 86:6445–6448.
- Seul, M., and J. Sammon. 1990. Competing interactions and domain-shape instabilities in a monomolecular film at an air-water interface. *Phys. Rev. Lett.* 64:1903–1906.
- Subramaniam, S., and H. M. McConnell. 1987. Critical mixing in monolayer mixtures of phospholipid and cholesterol. *J. Phys. Chem.* 91:1715–1718.
- Vist, M. R., and J. H. Davis. 1990. Phase equilibria of cholesterol/dipalmitoylphosphatidylcholine mixtures: ^2H nuclear magnetic resonance and differential scanning calorimetry. *Biochemistry.* 29:451–464.
- Vogel, V., and D. Möbius. 1988. Hydrated polar groups in lipid monolayers: effective local dipole moments and dielectric properties. *Thin Solid Films.* 159:73–81.
- Wisnieski, B. J., and C. F. Fox. 1976. Correlation between physical state and physiological activities in eukaryotic membranes, especially in response to temperature. In *The Molecular Basis of Circadian Rhythm*. Dahlem Konferenzem, Berlin. 247–266.